Applied Catalysis B: Environmental 98 (2010) 204–212

Contents lists available at ScienceDirect

Applied Catalysis B: Environmental

journal homepage: www.elsevier.com/locate/apcatb

Preferential oxidation of CO in H_2-rich stream over $CuO/Ce_{1-x}Ti_xO_2$ catalysts

Zhiwei Wu[a,b], Huaqing Zhu[a], Zhangfeng Qin[a], Hui Wang[a], Lichun Huang[a,b], Jianguo Wang[a,*]

[a] State Key Laboratory of Coal Conversion, Institute of Coal Chemistry, Chinese Academy of Sciences, P.O. Box 165, Taiyuan, Shanxi 030001, PR China
[b] Graduate University of the Chinese Academy of Sciences, Beijing 100049, PR China

ARTICLE INFO

Article history:
Received 12 February 2010
Received in revised form 27 May 2010
Accepted 31 May 2010
Available online 4 June 2010

Keywords:
CO preferential oxidation (PROX)
CuO catalyst
CeO_2
TiO_2
Sol–gel method

ABSTRACT

$CuO/Ce_{1-x}Ti_xO_2$ prepared by sol–gel impregnation was used as catalysts for the preferential oxidation (PROX) of CO in H_2-rich stream. The effects of support composition, catalyst calcination temperature as well as the presence of H_2O and CO_2 in the reaction stream on the catalytic performance of $CuO/Ce_{1-x}Ti_xO_2$ were investigated. The results indicated that the catalyst $CuO/Ce_{0.8}Ti_{0.2}O_2$ exhibits the highest activity and the optimal temperature for the catalyst calcination is 500 °C. The presence of H_2O and CO_2 in the reaction stream has a negative effect on the catalytic activity and stability of $CuO/Ce_{0.8}Ti_{0.2}O_2$. The negative effect of CO_2 on the catalyst stability is stronger than that of H_2O, suggesting that the accumulation of carbonate species may be the main reason for catalyst deactivation. The characterization by means of XRD, HRTEM, and H_2-TPR indicated that the doping of TiO_2 in CeO_2 enhances the surface area of the composite oxide support, decreases its particle size, and promotes the dispersion of active copper species. The strong interaction between TiO_2 and CeO_2 in the support as well as the interfacial interaction between CuO and the support may also contribute to the high catalytic activity of $CuO/Ce_{0.8}Ti_{0.2}O_2$.

1. Introduction

With the intense development of low temperature proton-exchange membrane fuel cell (PEMFC), the preferential oxidation (PROX) for removing trace amounts of CO from H_2-rich stream to avoid anode poisoning has attracted extensive attention in the past decades. A number of catalysts have been developed for the CO PROX reaction, which include the noble metal-based catalysts (Pt, Pd, Ru, Rh) [1–4], gold-based catalyst [5–8], and transition metal-based catalysts (Co, Cu, Mn) [9–11]. The platinum-group metals catalysts have desirable activity and stability at 150–200 °C, but they are not selective enough in the presence of H_2O and CO_2 [12]. Gold-based catalysts are more active than platinum-group metal catalysts at relatively low temperatures [13,14]. However, the transportation application of the noble metal-based catalysts may be limited by their high cost. Compared with the noble metal-based catalysts, the mixed oxide $CuO–CeO_2$ is very attractive for CO PROX due to its excellent performances and low cost [15–17]. It is more active and selective than Pt-group-based catalysts at low temperature [18] and also more selective and stable than the gold catalysts. For the industrial application, on the other side, the catalyst should have high stability and durability to the presence of H_2O and CO_2, because the reformate H_2-rich stream underwent a water–gas shift reaction contains 15–25 vol.% CO_2 and about 10 vol.% H_2O. However, $CuO–CeO_2$ is susceptible to the presence of CO_2 and H_2O in the reactant stream [19–21]. When the feed stream contains 10–25 vol.% H_2O and 10–25 vol.% CO_2, the temperature window for CO conversion above 99.0% is very narrow (about 5–20 °C) [12,22,23].

The redox behavior of cerium oxide can be modified by incorporation of other elements and the formation of mixed oxides. The capability of the redox couple $Ce^{4+}–Ce^{3+}$ is strongly enhanced if other elements are introduced into the CeO_2 lattice by forming solid solutions [24–27]. Lin et al. [24] reported that a synergistic interaction between CuO and $Ce_{0.7}Sn_{0.3}O_2$ makes the reduced $CuO/Ce_{0.7}Sn_{0.3}O_2$ catalyst be easily oxidized, which is responsible for the high CO oxidation activity at low temperature. Chen et al. [25] reported that the incorporation of Sn^{4+} into CeO_2 in the $CuO/Ce_xSn_{1-x}O_2$ catalysts promoted the selective oxidation of CO. They also found that an appropriate amount of zirconium ($1-x=0.1$) incorporated into CeO_2 for $CuO/Ce_xZr_{1-x}O_2$ and $CuO/Ce_xZr_{1-x}O_2$-Al_2O_3 catalysts could not only increase the mobility of lattice oxygen but also promote the activity of selective CO oxidation; when the amount of Zr^{4+} exceeded 10% ($1-x>0.1$), however, this promotion effect on CO oxidation was weakened [26,27].

The doping of ceria with other elements did not always enhance the activity of CuO-CeO_2 catalyst in CO oxidation. Ratnasamy et al. [28] investigated the CO PROX activity of CuO-CeO_2, CuO-CeO_2-ZrO_2 and CuO-ZrO_2 catalysts prepared by coprecipitation method; they observed that CuO-CeO_2 exhibited superior activity than CuO-CeO_2-ZrO_2 and CuO-ZrO_2. Martínez-Arias et al. [29] revealed that

* Corresponding author. Tel.: +86 351 4046092; fax: +86 351 4041153.
E-mail address: iccjgw@sxicc.ac.cn (J. Wang).

0926-3373/$ – see front matter © 2010 Elsevier B.V. All rights reserved.
doi:10.1016/j.apcatb.2010.05.030

$CuO/Ce\text{-}M\text{-}O_2$ catalyst (M = Zr, Tb) prepared by precipitation using a reverse microemulsion method exhibited inferior activity to the CuO/CeO_2 catalyst. Manzoli et al. [30] and Caputo et al. [31] also found that doping cerium with zirconia has no beneficial effect on CO PROX performance. The inconsistent conclusion may be originated from the different methods for preparing catalysts and the various doping elements. However, we can still get a rough estimation that the $CuO/Ce_{1-x}M_xO_2$ catalysts with low level cerium doping ($x \leq 0.3$) show better CO PROX performance than the heavy doping ones ($x \geq 0.5$), especially for the cerium-containing catalysts doped with zirconia [26,31].

The incorporation of Ti into CeO_2 can significantly improve the storage capacity of mobile oxygen of CeO_2 [32]. In this respect, the Ce–Ti–O composite oxides were prepared and investigated as promising supports [32–34]. The catalysts supported on the Ce–Ti–O composite oxides have been used in the reactions such as stream forming of ethanol [35], partial oxidation of methane [36], oxidation of volatile organic compounds (VOCs) [37], and photocatalytic degradation of chlorophenol [38]. We also found that Pd supported on the ceria–titania composite oxides (Pd/CeO_2–TiO_2) prepared by sol–gel precipitation followed by supercritical fluid dry (SCFD) exhibited high activity for CO oxidation at low temperature [39]. The temperature-programmed reduction (TPR) using H_2 and CO as reducing agents suggested that the Pd–Ce interaction in Pd/CeO_2–TiO_2 favored the reduction of both PdO and CeO_2, which contributed to the high activity for CO oxidation at low temperature [40–42]. The pretreatments of calcination and reduction exhibited significant effects on the catalytic behavior of Pd/CeO_2-TiO_2 [43,44]. Moreover, Pd/CeO_2-TiO_2 can still perform well in CO oxidation under the relatively actual conditions in the presence of H_2O and CO_2 [45,46]. Recently, Sangeetha and Chen reported that Au/CeO_2–TiO_2 exhibited high activity in the CO PROX reaction at low temperature [47]. It is then supposed that the modified oxygen storage capacity of CeO_2 by TiO_2 may also promote the activity of supported Cu species for CO oxidation in H_2-rich stream. However, as far as we know, copper supported on Ce–Ti–O composite oxides used for CO PROX was scarcely reported.

Therefore, in this work, the $CuO/Ce_{1-x}Ti_xO_2$ catalysts with various Ti/(Ce + Ti) atomic ratios were prepared by sol–gel impregnation. The effects of support composition, catalyst calcination temperature as well as the presence of H_2O and CO_2 in the reaction stream on the catalytic performance of $CuO/Ce_{1-x}Ti_xO_2$ for CO PROX in H_2-rich stream were investigated.

2. Experimental

2.1. Catalyst preparation

CeO_2, TiO_2 and $Ce_{1-x}Ti_xO_2$ composite oxides were prepared by sol–gel precipitation method at room temperature as described elsewhere [39,40]. Briefly, the alcosol was obtained through the hydrolysis of $Ce(NO_3)_3{\cdot}6H_2O$ and $Ti(SO_4)_2$ in ethanol under stirring. The precipitation was achieved with the solution of $NH_3{\cdot}H_2O$ at ambient temperature. After aging and filtration, the precipitate was washed with deionized water until no SO_4^{2+} ions were detected with $Ba(NO_3)_2$ solution. To drive out of the water in the wet precipitate, the material was then washed with ethanol. The resulting alcogel was dried at 110 °C and finally calcined at 500 °C in air for 4 h.

CuO-supported catalysts were prepared by the incipient wetness impregnation method with aqueous $Cu(NO_3)_2$ solution. The catalyst was then dried at 110 °C for 12 h and calcined in air at the temperature of 400–800 °C for 4 h. The nominal value of Ti/(Ce + Ti) atomic ratios (x) was in the range of 0–1 for the $Ce_{1-x}Ti_xO_2$ composite oxides, and the CuO loading was 10.0 wt.% for the $CuO/Ce_{1-x}Ti_xO_2$ catalysts.

2.2. Catalyst characterization

The powder X-ray diffraction (XRD) was performed on an advanced X-ray diffractometer (Bruker AXS D8, Germany). The diffraction patterns of the samples were recorded at room temperature with Cu Kα radiation (154.06 pm, 40 kV, and 40 mA) in the range of 2θ between 10° and 90°. The average crystallite size was estimated from the line broadening of the most intense XRD reflections with Scherrer formula, and the cell parameter of cubic CeO_2 is obtained by the MDI Jade5 software.

The Brunauer–Emmett–Teller (BET) surface area of the catalysts was measured by nitrogen adsorption at −195.8 °C with a TriStar 3000 Gas Absorption Analyzer (Micromeritics Instrument Co., USA). The samples were degassed at 200 °C and 6.7 Pa for 2 h prior to the measurement.

The high-resolution transmission electron microscopy (HRTEM) images of the samples were obtained using a JEM 2010 microscope operating at 200 kV and equipped with an energy-dispersive X-ray (EDX) instrument. The catalyst was crushed to a fine powder, and then a holey carbon film copper grid was dipped into the crushed powder. The mean particle size is estimated from a statistic result of 100 particles randomly selected in TEM images.

The temperature-programmed reduction of H_2 (H_2-TPR) was performed in a quartz microreactor, and 50 mg sample was used in each measurement as described elsewhere [40,41]. The samples were first pretreated under an air flow (30 ml/min) at 300 °C for 1 h, followed by purging with Ar (30 ml/min) at the same temperature for 1 h and then cooled down to room temperature (RT). After that, a flow of 5% H_2 in Ar (30 ml/min) was switched into the system and the sample was heated up to 700 °C from room temperature at a rate of 10 °C/min. The amount of H_2 uptake during the reduction was measured by a thermal conductivity detector (TCD), which was calibrated by the quantitative reduction of a given amount of CuO to the metallic copper.

2.3. Catalytic tests and analytical procedure

The catalytic test for CO PROX in a hydrogen-rich stream was carried out in a quartz tubular flow microreactor with an internal diameter of 6.0 mm at atmospheric pressure as described previously [7,8]. The reacting stream consisted of 1.0% CO (by volume, hereinafter), 1% O_2, 50% H_2, 10% H_2O (when used), 15% CO_2 (when used), and balanced N_2. H_2O was introduced to the feed through a bubbler saturator. The total flow rate is 100 ml/min, and the weight of the catalyst used in each run is 500–200 mg, corresponding to a space velocity of 12,000–60,000 ml g^{-1} h^{-1}. The catalyst bed was about 1.0–2.5 cm in height and placed in the constant temperature zone (3–4 cm high) of the microreactor. Before the light-off tests, the catalyst was pretreated at 300 °C for 1 h in air with a flow rate of 30 ml/min. Then the catalytic reaction was performed from room temperature up to 200 °C at a heating rate of 2 °C/min.

CO, CO_2 and O_2 in the reaction stream and effluent were analyzed online with gas chromatographs as described elsewhere [7,8]. CO conversion was determined either based on CO_2 formation or CO consumption (when excess CO_2 was added):

$$\text{CO conversion}\,(x_{CO}) = \frac{[CO_2]_{out}}{[CO]_{out} + [CO_2]_{out}} \times 100\%\ \text{or}$$

$$\text{CO conversion}\,(x_{CO}) = \frac{[CO]_{in} - [CO]_{out}}{[CO]_{in}} \times 100\%\ (\text{when excess } CO_2 \text{ was added}).$$

O_2 conversion was determined from the O_2 concentrations in the reactant gas and in the effluent gas and the selectivity of CO PROX (CO_2 selectivity) was defined as the fraction of O_2 consumption for the CO oxidation to CO_2 over the total O_2 consumption:

$$O_2\ \text{conversion}\ (x_{O_2}) = \frac{[O_2]_{in} - [O_2]_{out}}{[O_2]_{in}} \times 100\%\ \text{and}$$

$$CO_2\ \text{selectivity}\ (S_{CO_2}) = x_{CO} \times \frac{[CO]_{in}}{2x_{O_2} \times [O_2]_{in}} \times 100\%.$$

3. Results and discussion

3.1. Catalytic performance

3.1.1. Effect of Ti/(Ce + Ti) atomic ratio on the catalyst performance

Fig. 1 shows the CO conversion and CO_2 selectivity for CO PROX on $CuO/Ce_{1-x}Ti_xO_2$ catalysts with different Ti/(Ce + Ti) atomic ratios (x) in the reacting stream containing 1 vol.% CO, 1 vol.% O_2, 50 vol.% H_2, and balanced N_2. The temperature window for effective CO removal ($T_{99.5}$, where the CO conversion is above 99.5%, namely the residual CO is 50 ppm in the outlet flow) and the corresponding maximum CO_2 selectivity (at this temperature zone) are summarized in Table 1. CuO/CeO_2 exhibits high activity for CO PROX with $T_{99.5}$ being 110–180 °C and the maximum CO_2 selectivity in this region is 98.7% at 110 °C. Over CuO/TiO_2, CO cannot be fully converted under the temperature region tested; the maximum CO conversion is 85.7% at 180 °C with CO_2 selectivity of 47.0%. In general, $CuO/Ce_{1-x}Ti_xO_2$ is less active than CuO/CeO_2 but more active than CuO/TiO_2. However, when x is 0.2, the catalyst $CuO/Ce_{0.8}Ti_{0.2}O_2$ exhibits much higher activity than CuO/CeO_2 and other catalysts tested. Over the $CuO/Ce_{0.8}Ti_{0.2}O_2$ catalyst, CO can be completely converted at lower temperature with a wider temperature window of 90–170 °C, with the maximum CO_2 selectivity being 100% at 90 °C.

Table 1
Temperature window for the effective CO removal ($T_{99.5}$, with CO conversion ≥99.5%) and the maximum CO_2 selectivity (S_{max}) in CO PROX at $T_{99.5}$ over $CuO/Ce_{1-x}Ti_xO_2$ catalysts with different Ti/(Ce + Ti) atomic ratios calcined at 500 °C.

Samples	$T_{99.5}$ window (°C)	S_{max} (%)
CuO/CeO_2	110–180	98.7
$CuO/Ce_{0.8}Ti_{0.2}O_2$	90–170	100.0
$CuO/Ce_{0.6}Ti_{0.4}O_2$	120–150	91.1
$CuO/Ce_{0.4}Ti_{0.6}O_2$	140–160	75.4
$CuO/Ce_{0.2}Ti_{0.8}O_2$	140	60.0
CuO/TiO_2	180[a]	47.0

[a] Temperature corresponds to the maximum CO conversion.

3.1.2. Effects of H_2O and CO_2 in the feed on the CO PROX behavior

As the $CuO/Ce_{0.8}Ti_{0.2}O_2$ catalyst performs best among the tested samples, the influence of H_2O and CO_2 on its catalytic behavior is investigated and the results are shown in Fig. 2. The presence of CO_2 and H_2O causes a sharp decrease in the CO PROX activity and narrows the temperature window for CO effective removal. When the feed stream is free of CO_2 and H_2O, CO can be effectively removed at 90–170 °C with the maximum CO_2 selectivity being 100% at 90 °C. When 10% H_2O is added to the feed stream, CO can only be effectively removed in the region of 130–170 °C and the maximum CO_2 selectivity is 95.1%. While 10% H_2O and 15% CO_2 are simultaneously present in the reaction stream, the negative effect of H_2O and CO_2 on the catalytic performance of $CuO/Ce_{0.8}Ti_{0.2}O_2$ is aggravated: CO can only be effectively removed in the region of 140–170 °C with the maximum CO_2 selectivity of 84.5%. To reach the same CO conversion when both CO_2 and H_2O are present in the feed, the reaction temperature must be raised by about 40–50 °C; the CO_2 selectivity becomes lower. Park et al. [48] assumed that the negative effect of CO_2 on the catalytic performance is related to the competitive adsorption of CO and CO_2 on the catalyst surface, while Gamarra and Martínez-Arias [49] supposed that the catalyst deactivation induced by CO_2 was mainly related to the modification of interfacial sites upon the formation of specific carbonates. The decrease of catalytic activity with H_2O in the reactant feed is mainly ascribed to the blockage of the active sites by the molecular water adsorbed [48,49].

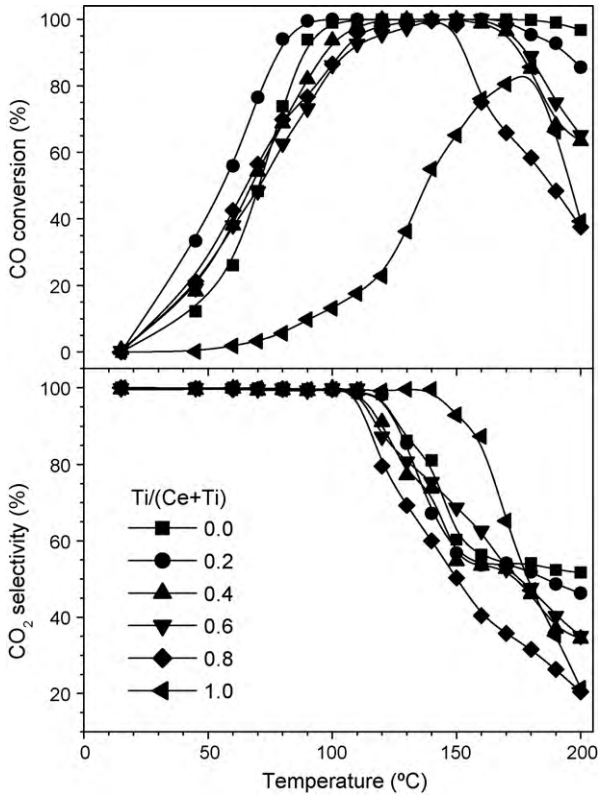

Fig. 1. Temperature-programmed reaction curves of CO PROX over $CuO/Ce_{1-x}Ti_xO_2$ catalysts calcined at 500 °C with different Ti/(Ce + Ti) atomic ratios (x). Reaction conditions: 1% CO, 1% O_2, 50% H_2, and balanced N_2; SV = 30,000 ml g^{-1} h^{-1}.

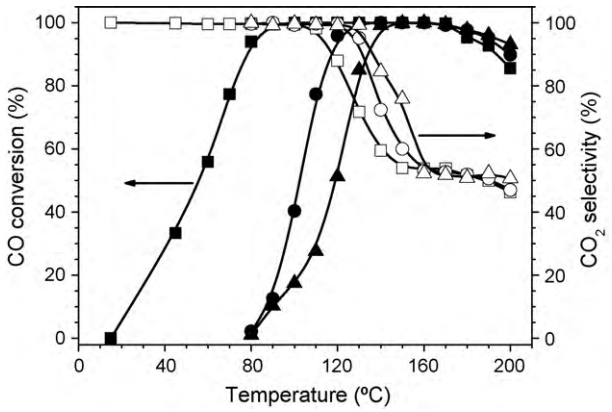

Fig. 2. Temperature-programmed reaction curves of CO PROX over $CuO/Ce_{0.8}Ti_{0.2}O_2$ catalysts calcined at 500 °C in different feed streams: (■, □) (1% CO + 1% O_2 + 50% H_2)/N_2; (●, ○) (1% CO + 1% O_2 + 10% H_2O + 50% H_2)/N_2; (▲, △) (1% CO + 1% O_2 + 10% H_2O + 15% CO_2 + 50% H_2)/N_2. SV = 30,000 ml g^{-1} h^{-1}.

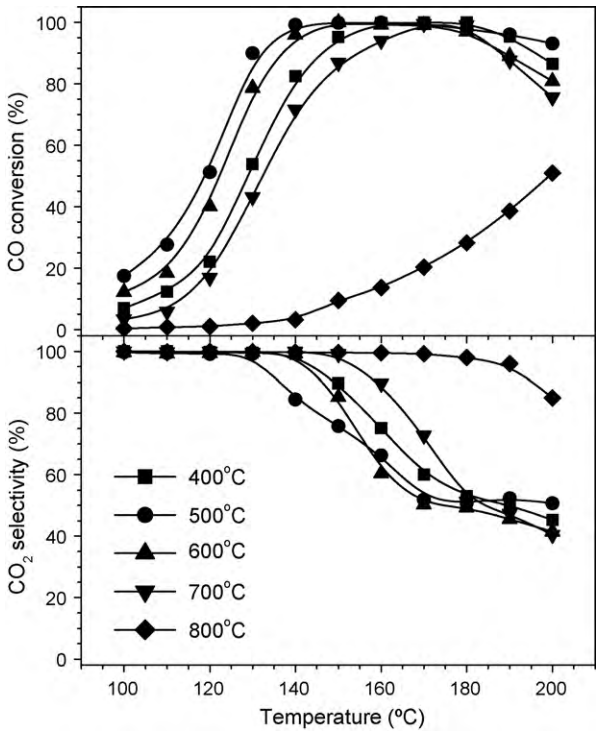

Fig. 3. Temperature-programmed reaction curves of CO PROX over $CuO/Ce_{0.8}Ti_{0.2}O_2$ catalysts with different calcination temperatures. Reaction conditions: 1% CO, 1% O_2, 10% H_2O, 15% CO_2, 50% H_2, and balanced N_2; SV = 30,000 ml g^{-1} h^{-1}.

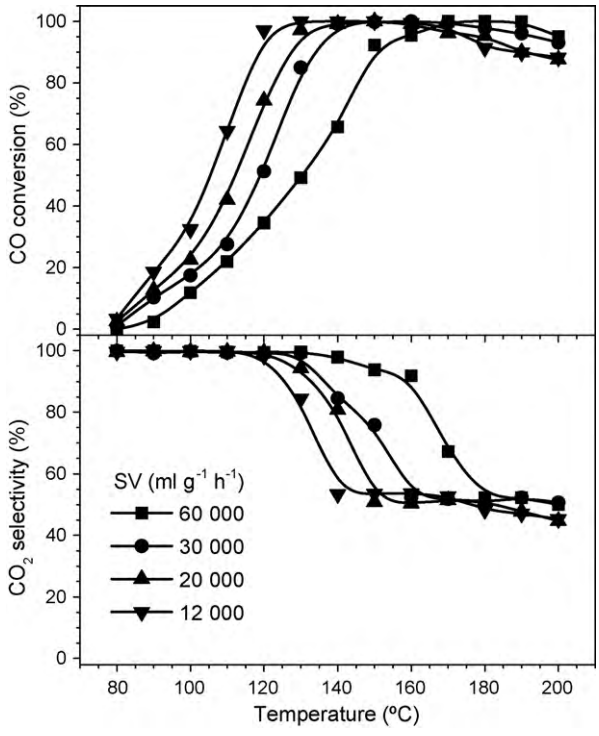

Fig. 4. Temperature-programmed reaction of CO PROX over $CuO/Ce_{0.8}Ti_{0.2}O_2$ catalysts calcined at 500 °C at different space velocities. Reaction conditions: 1% CO, 1% O_2, 10% H_2O, 15% CO_2, 50% H_2, and balanced N_2.

3.1.3. *Effect of calcination temperature on the catalyst performance*

Fig. 3 shows the results of CO PROX over the $CuO/Ce_{0.8}Ti_{0.2}O_2$ catalysts calcined at different temperatures with 10 vol.% H_2O and 15 vol.% CO_2 in the feed. The best catalyst performance is obtained upon calcination at 500 °C (T_{500}). The activity of the catalysts prepared is in the order: $T_{500} > T_{600} > T_{400} > T_{700} > T_{800}$, while the selectivity is almost in a reverse order.

3.1.4. *Effect of space velocity on CO PROX*

The effect of the space velocity on CO PROX behavior over the catalyst $CuO/Ce_{0.8}Ti_{0.2}O_2$ (calcined at 500 °C) is shown in Fig. 4. As expected, the CO conversion decreases with the increase of the space velocity from 12,000 to 60,000 ml g^{-1} h^{-1}.

3.1.5. *Stability of $CuO/Ce_{0.8}Ti_{0.2}O_2$ catalyst*

The long-term test for CO PROX over the $CuO/Ce_{0.8}Ti_{0.2}O_2$ catalyst in different streams is shown in Fig. 5. When no extra H_2O and CO_2 are added in the feed (Fig. 5A), the catalyst exhibits good stability with nearly 100% CO conversion and about 100% CO_2 selectivity for 240 h at 90 °C. However, the same CO conversion cannot be obtained even at 120 °C when 10% H_2O is present in the reaction stream (Fig. 5B). Moreover, the raising of reaction temperature leads to a slight drop of the CO_2 selectivity to about 95.0%, indicating the onset of hydrogen oxidation. Nevertheless, no obvious decrease of CO conversion and CO_2 selectivity is found during the 240 h test.

When 15% CO_2 is added to the reaction stream (Fig. 5C), the test is also performed at 120 °C to maintain the initial CO conversion being 100%. Hence the conversion of CO decreases gradually from about 100% to 95.9% with the CO_2 selectivity of about 98% in the first 100 h, indicating a catalyst deactivation. Raising the reaction temperature to 130 °C can recover the CO conversion to 99.6% at the beginning, but the catalyst deactivation is also accelerated in the subsequent 100 h on stream. The conversion of CO can be recovered to 99.1% with an in situ regeneration treatment in air flow at 300 °C for 2 h; afterward, however, it drops quickly to 92.7% in the following 40 h. The presence of both 10% H_2O and 15% CO_2 in the reaction stream (Fig. 5D) shows the similar effect on the catalytic performance as that of CO_2, except that the reaction temperature should be raised by another 10 °C to reach the same initial CO conversion.

For the Cu-based catalyst, Kim and Cha [19] proposed that the accumulation of carbonate species is the main cause of the catalyst deactivation for CO PROX with CO_2 and H_2O in the reactant stream, while the initial activity can be easily recovered upon a treatment at 300 °C with different atmospheres (O_2, H_2, and He). Sedmak et al. [50] attributed the catalyst deactivation to the redistribution of some copper species. Based on the DRIFTS study, Martínez-Arias et al. [51] suggested that the accumulation of hydroxyl species at CuO-CeO_2 interfacial active sites may be the main reason for the catalyst deactivation.

Current results also indicate that H_2O and CO_2 are different in their effects on the catalyst stability. Although the presence of H_2O in the reaction stream increases the temperature for a certain CO conversion, it has little influence on the catalyst stability. To counteract the competitive adsorption of H_2O on the catalyst surface, the reaction temperature should be raised to achieve the same CO conversion as that without adding additional H_2O. On the other hand, the stability of the catalyst $CuO/Ce_{0.8}Ti_{0.2}O_2$ is deteriorated by the presence of CO_2 in the reaction stream. The addition of CO_2 in the feed not only leads to a significant increase of the reaction temperature for a given CO conversion, but also causes a remarkable deactivation of the catalyst. The negative effect of CO_2 on the stability of the catalyst $CuO/Ce_{0.8}Ti_{0.2}O_2$ in CO PROX is stronger than that of H_2O, suggesting that the accumulation of carbonate species may be the main reason for the catalyst deactivation.

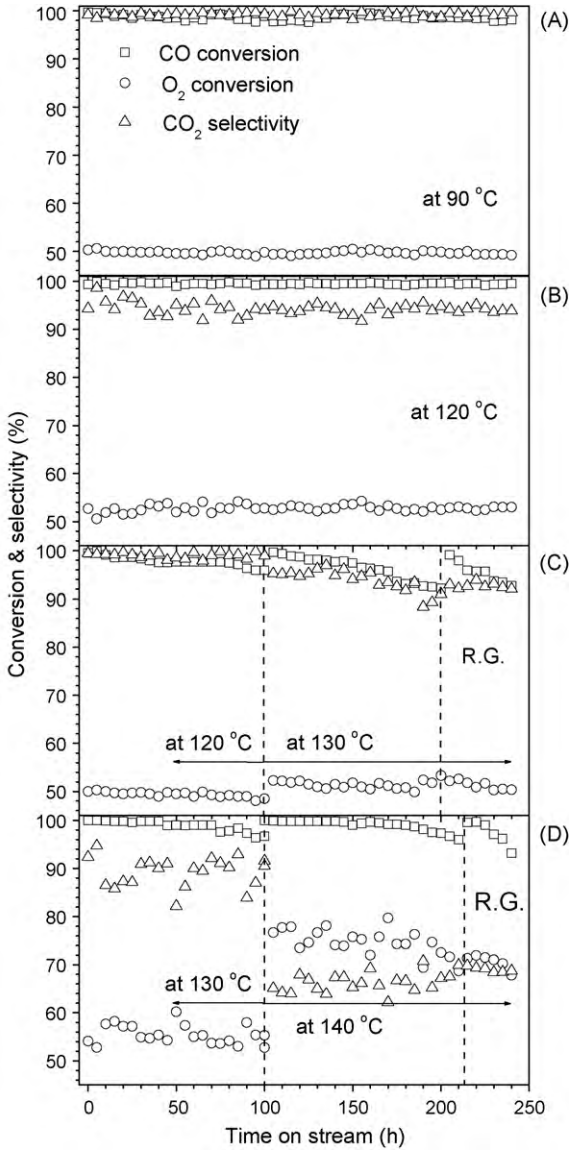

Fig. 5. Long-term test of CO PROX over the catalyst $CuO/Ce_{0.8}Ti_{0.2}O_2$ calcined at 500 °C in the reaction stream of (1% CO + 1% O_2 + 50% H_2)/N_2 (A) without H_2O and CO_2, (B) with 10% H_2O, (C) with 15% CO_2, and (D) with 10% H_2O + 15% CO_2. SV = 12,000 ml g^{-1} h^{-1} (R.G. represents an in situ regeneration in air at 300 °C for 1 h.).

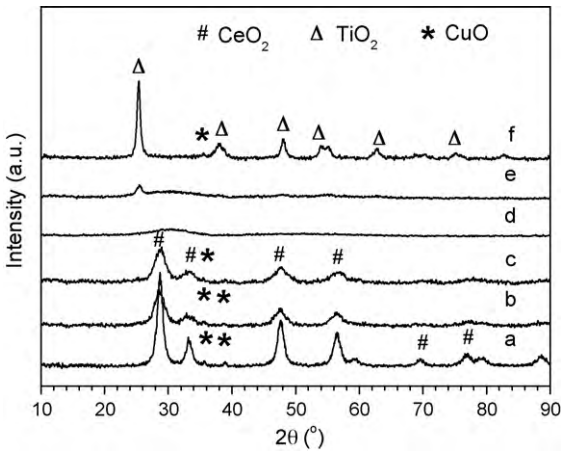

Fig. 6. XRD patterns of the CuO catalysts calcined at 500 °C supported on (a) CeO_2, (b) $Ce_{0.8}Ti_{0.2}O_2$, (c) $Ce_{0.6}Ti_{0.4}O_2$, (d) $Ce_{0.4}Ti_{0.6}O_2$, (e) $Ce_{0.2}Ti_{0.8}O_2$, and (f) TiO_2.

3.2. Catalyst characterization

3.2.1. XRD and BET surface area

The specific surface area and particle size of the $CuO/Ce_{1-x}Ti_xO_2$ catalysts with different Ti/(Ce + Ti) ratios (x), estimated by N_2 sorption, XRD and TEM measurements, are listed in Table 2. The catalysts CuO supported on $Ce_{1-x}Ti_xO_2$ composite oxide exhibit higher surface area than CuO/CeO_2 and CuO/TiO_2.

As shown by the XRD patterns in Fig. 6, typical fluorite and anatase phases are observed in CuO/CeO_2 and CuO/TiO_2, respectively, while a phase transition from fluorite to anatase is detected in the $CuO/Ce_{1-x}Ti_xO_2$ catalysts with the increase of Ti/(Ce + Ti) ratio. When x is below 0.4, cerianite phase of CeO_2 is observed in the catalysts. Compared with CuO/CeO_2, the diffraction peaks of fluorite CeO_2 in $CuO/Ce_{0.8}Ti_{0.2}O_2$ becomes wider, indicating that the doping of TiO_2 makes the crystallite size of CeO_2 smaller. As listed in Table 2, the cell parameter of cubic CeO_2 (1 1 1) plane in the catalyst $CuO/Ce_{0.8}Ti_{0.2}O_2$ is smaller than that in CuO/CeO_2.

The similar phenomena have been observed in ceria-related mixed oxides [29,32,52]. A solid solution is formed through the entrance of a portion of Ti^{4+} ions into the lattice of CeO_2 [40,41,53], because the radius of Ti^{4+} (0.068 nm) are smaller than that of Ce^{3+} (0.103 nm) and Ce^{4+} (0.099 nm). However, further increase of x to 0.4 leads to little change in the CeO_2 crystallite size. It seems that an excess doping of TiO_2 is not favorable for the formation of the solid solution. Probably, only a low content of Ti ($x \leq 0.2$) can be incorporated into the lattice of CeO_2; excess Ti cations cannot enter the lattice of CeO_2 and even turn to be an obstacle to the formation of the solid solution. When x is increased to 0.6, no obvious crystallite phase can be detected. The anatase phase of TiO_2 is not detected until x is increased to 0.8, indicating that TiO_2 is present as amorphous phase when x is below 0.8. Compared with CuO/TiO_2, only the (1 0 1) plane of anatase phase is detected in the catalyst with x being 0.8; it suggests that a small amount of CeO_2 added to TiO_2 will significantly suppress the formation of TiO_2 crystallite phase.

CuO tenorite phase can be clearly observed in CuO/CeO_2 and CuO/TiO_2 catalysts. However, the intensity of CuO diffraction peaks is very weak in the catalysts $CuO/Ce_{0.8}Ti_{0.2}O_2$ and $CuO/Ce_{0.6}Ti_{0.4}O_2$. The signals of CuO are even faded out in the catalysts $CuO/Ce_{0.4}Ti_{0.6}O_2$ and $CuO/Ce_{0.2}Ti_{0.8}O_2$. These suggest that CuO species is highly dispersed on the catalysts $CuO/Ce_{1-x}Ti_xO_2$ (especially on $CuO/Ce_{0.4}Ti_{0.6}O_2$ and $CuO/Ce_{0.2}Ti_{0.8}O_2$ with high surface area).

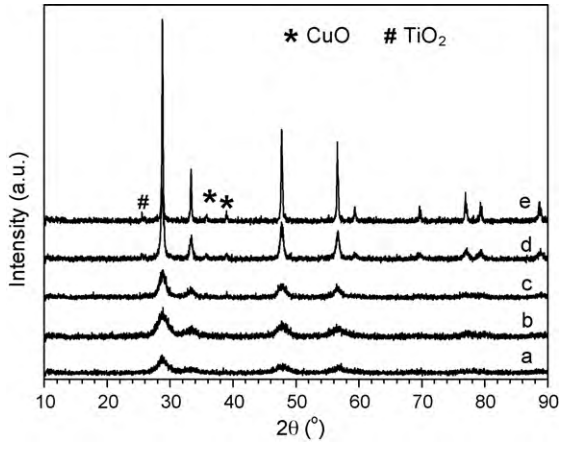

Fig. 7. XRD patterns of the catalysts $CuO/Ce_{0.8}Ti_{0.2}O_2$ calcined at (a) 400, (b) 500, (c) 600, (d) 700, and (e) 800 °C.

Table 2
Specific surface area, crystallite size (d) of CeO_2 and TiO_2 phases, and mean particle size of $CuO/Ce_{1-x}Ti_xO_2$ catalysts calcined at 500 °C.

Samples	S_{BET} (m^2/g)	Crystallite size from XRD (nm)		CeO_2 cell parameter from XRD (nm)	Particle size from TEM (nm)
		d_{CeO_2}	d_{TiO_2}		
CuO/CeO_2	82.0	8.6	–	0.5415	6.7
$CuO/Ce_{0.8}Ti_{0.2}O_2$	103.0	5.0	–	0.5398	6.1
$CuO/Ce_{0.6}Ti_{0.4}O_2$	102.6	5.2	–	0.5401	6.0
$CuO/Ce_{0.4}Ti_{0.6}O_2$	138.6	–	–	–	5.0
$CuO/Ce_{0.2}Ti_{0.8}O_2$	131.0	–	8.2	–	5.4
CuO/TiO_2	53.4	–	15.3	–	14.6

Table 3
Specific surface area and XRD results of $CuO/Ce_{0.8}Ti_{0.2}O_2$ catalysts calcined at different temperatures.

Calcination temperature (°C)	S_{BET} (m^2/g)	d_{CeO_2} (nm)	CeO_2 cell parameter (nm)
400	120.9	4.9	0.5407
500	103.0	5.0	0.5398
600	45.8	7.2	0.5399
700	16.5	15.4	0.5410
800	2.9	59.5	0.5406

Fig. 7 shows the XRD patterns of $CuO/Ce_{0.8}Ti_{0.2}O_2$ catalysts calcined at different temperatures. Their BET surface area and XRD analysis results are summarized in Table 3. The major diffraction peaks are ascribed to fluorite CeO_2 phase. With the increase of the calcination temperature from 400 to 800 °C, the crystallite size of CeO_2 grows up severely from 4.3 to 59.5 nm, accompanied with a sharp decrease of the specific surface area from 120.9 to 2.9 m^2/g. CuO phase in the catalysts can be detected when the calcination temperature exceeds 500 °C; its diffraction intensity is enhanced with the increase of the calcination temperature. It is obvious that the catalyst calcined at 500 °C exhibits the minimum CeO_2 cell parameter. The shrinkage of CeO_2 cell unit indicates the formation of a solid solution through the entrance of smaller Cu^{2+} (0.062 nm) and/or Ti^{4+} (0.068 nm) ions into the lattice of CeO_2. However, high calcination temperature (≥700 °C) may destroy the structure of the solid solution and get back the cell parameter of the lattice of CeO_2. It is probably correlated with the segregation of TiO_2 and CuO, as shown by the XRD patterns of the catalyst calcined at a temperature higher than 700 °C. It may reflect a fact that high calcination temperature will provide the power to push out the Ti^{4+} or Cu^{2+} from the lattice of CeO_2. As a result, the temperature above 700 °C is not favorable for the formation of a solid solution, similar to that observed by Dong et al. [54]. The change in CeO_2 cell parameter upon calcination suggests that 500 °C is the optimal calcination temperature for the formation of TiO_2–CeO_2 solid solution.

3.2.2. HRTEM

The mean particle sizes of the catalysts obtained from the TEM images are listed in Table 2. The particle sizes are in the same magnification scale as the crystallite sizes estimated from XRD analysis. Similar to those obtained from XRD results, the catalysts CuO supported on $Ce_{1-x}Ti_xO_2$ composite oxides have smaller particle sizes than CuO/CeO_2 and CuO/TiO_2.

The HRTEM images of $CuO/Ce_{1-x}Ti_xO_2$ catalysts with various Ti/(Ce + Ti) ratios are shown in Fig. 8. For CuO/CeO_2 catalyst, CeO_2 (1 1 1), CuO (1 1 1), and CuO (−1 1 1) planes are detected with the crystal spaces (d) of 0.310, 0.228, and 0.250 nm, respectively. For CuO/TiO_2 catalyst, TiO_2 (1 0 1) planes (d = 0.350 nm) and CuO planes can be observed. For $CuO/Ce_{1-x}Ti_xO_2$ catalysts, CeO_2 (1 1 1) planes are present both in $CuO/Ce_{0.8}Ti_{0.2}O_2$ and $CuO/Ce_{0.6}Ti_{0.4}O_2$. TiO_2 crystallite planes are not observed in these two catalysts but can be detected by EDX analysis, indicating that TiO_2 is present as very small particles or amorphous phase. CuO planes are observed in $CuO/Ce_{0.8}Ti_{0.2}O_2$, which is consistent with the XRD analysis; however, they are not detected in $CuO/Ce_{0.6}Ti_{0.4}O_2$, slightly different from the XRD result. It is supposed that CuO particles may be embedded in TiO_2 and CeO_2 and then becomes invisible on the surface by TEM but detectable in the bulk by XRD. In $CuO/Ce_{0.2}Ti_{0.8}O_2$ only TiO_2 (1 0 1) planes are observed, while in $CuO/Ce_{0.4}Ti_{0.6}O_2$ all phases are amorphous.

3.2.3. H_2-TPR

The H_2-TPR profiles of $CuO/Ce_{1-x}Ti_xO_2$ catalysts with different Ti/(Ce + Ti) atomic ratios along with the corresponding supports are shown in Fig. 9. The quantitative results are listed in Table 4. The H_2-TPR of CeO_2 shows a reduction peak centered at 494 °C, which is attributed to the reduction of the surface-capping oxygen of CeO_2, since the bulk CeO_2 is reduced at above 800 °C [40]. Assuming only Ce^{4+} ions are present in the CeO_2 sample, the H_2-TPR process reveals that 11.6% CeO_2 is reduced to Ce_2O_3 in the support. For TiO_2 support, a very small H_2-TPR peak centered at 549 °C is observed, which is ascribed to the reduction of surface oxygen of TiO_2. Comparing with CeO_2, the reduction of TiO_2 is more difficult and is here then negligible; therefore, the H_2 uptakes detected for $Ce_{1-x}Ti_xO_2$ composite oxides can

Table 4
H_2-TPR analysis of $CuO/Ce_{1-x}Ti_xO_2$ catalysts calcined at 500 °C and corresponding supports with Ti/(Ce + Ti) atomic ratio (x) ranging from 0 to 1.

x	$Ce_{1-x}Ti_xO_2$ supports		$CuO/Ce_{1-x}Ti_xO_2$ catalysts				CeO_2 content (μmol/g)		Reducible CeO_2 (%)[a]	
	Position (°C)	H_2 uptake (μmol/g)	α (°C)	β (°C)	γ (°C)	H_2 uptake (μmol/g)	Support	Catalyst	Support	Catalyst
0	494	337	144	166	223	1595	5811	5230	11.6	12.9
0.2	494	579	121	155	–	1761	5201	4686	22.2	21.5
0.4	487	1200	167	189	–	2429	4438	3994	54.1	58.7
0.6	500	1078	188	223	–	2423	3426	3083	62.9	75.6
0.8	520	768	188	211	–	1820	2034	1831	75.5	61.5
1	549	105	154	211	234	1388	12520[b]	11268[b]	1.7[c]	2.3[c]

[a] The reducible CeO_2 is the percentage of the reducible part of CeO_2 in the support or catalyst. For the supports $Ce_{1-x}Ti_xO_2$, it is determined by 2 × [total H_2 uptake]/[CeO_2 content] × 100%. For the catalysts $CuO/Ce_{1-x}Ti_xO_2$, it is determined by 2 × [total H_2 consumption − 1257]/[CeO_2 content] × 100%, where the value 1257 μmol/g is the H_2 uptake for the reduction of 10 wt.% CuO in the catalysts.
[b] The data denote the amount of TiO_2 in support or CuO/TiO_2 catalyst.
[c] The data denote the fraction of reducible TiO_2 in TiO_2 support or CuO/TiO_2 catalyst.

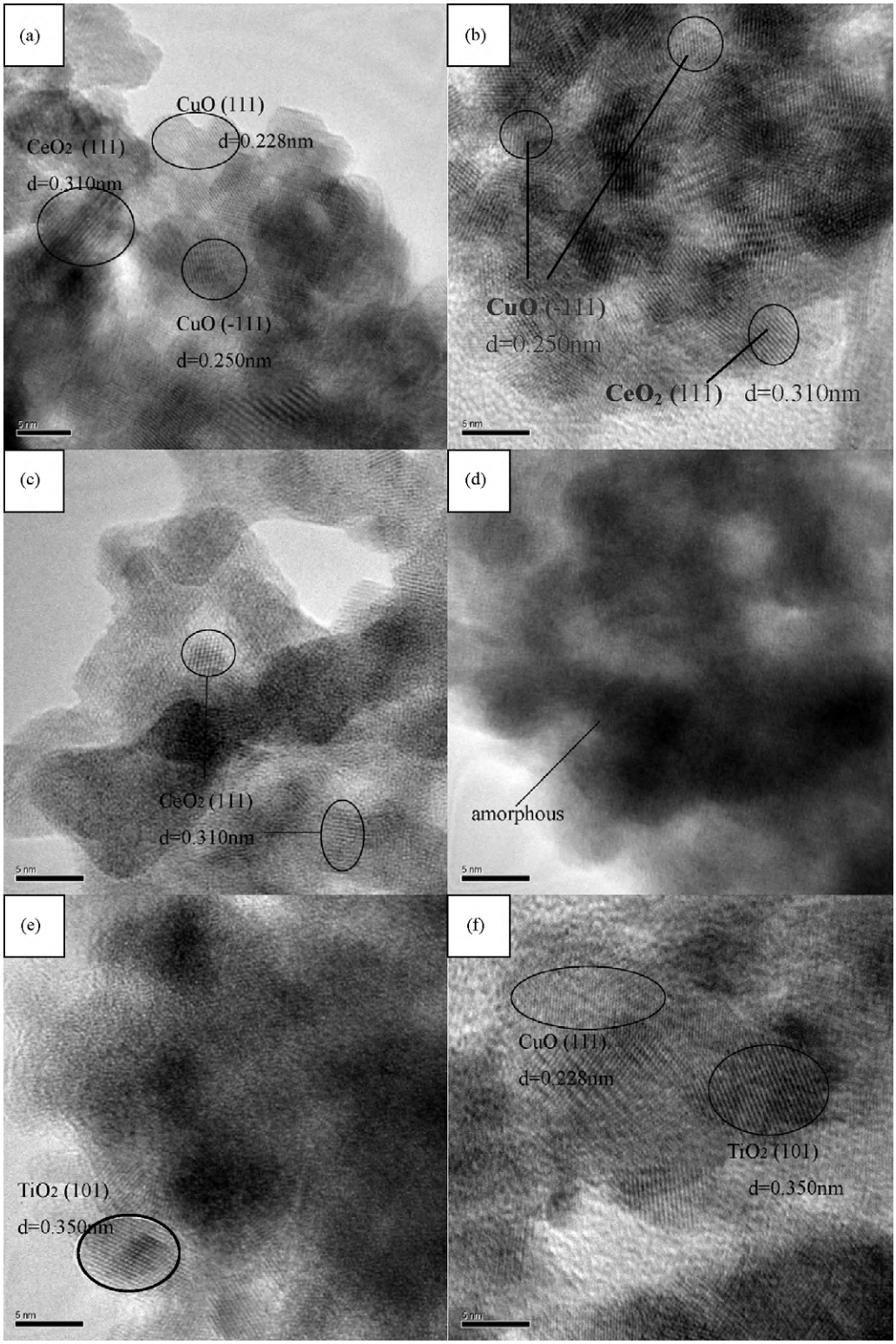

Fig. 8. HRTEM images of (a) CuO/CeO_2, (b) $CuO/Ce_{0.8}Ti_{0.2}O_2$, (c) $CuO/Ce_{0.6}Ti_{0.4}O_2$, (d) $CuO/Ce_{0.4}Ti_{0.6}O_2$, (e) $CuO/Ce_{0.2}Ti_{0.8}O_2$, and (f) CuO/TiO_2 calcined at 500 °C.

be mainly ascribed to the reduction of CeO_2. In most cases, the doping of TiO_2 into CeO_2 increases the reduction temperature of $Ce_{1-x}Ti_xO_2$ composite oxides, except for $Ce_{0.6}Ti_{0.4}O_2$, whose reduction temperature is slightly lower than that of pure CeO_2. However, the fraction of the reducible CeO_2 increases monotonously with the decrease of CeO_2 content and the increase of TiO_2 ratio in the supports, indicating that the interaction between TiO_2 and CeO_2 improves the mobility of oxygen and enhances the reduction of CeO_2.

In the H_2-TPR profile of CuO/CeO_2 catalyst, three reduction peaks (α, β, γ) are present at 144, 166, and 223 °C, respectively, while the H_2-TPR of CuO/TiO_2 shows the reduction peaks at 154, 211, and 234 °C. For $CuO/Ce_{1-x}Ti_xO_2$ catalysts with x being 0.2–0.8, the H_2-TPR profiles are only split into two separate peaks α and

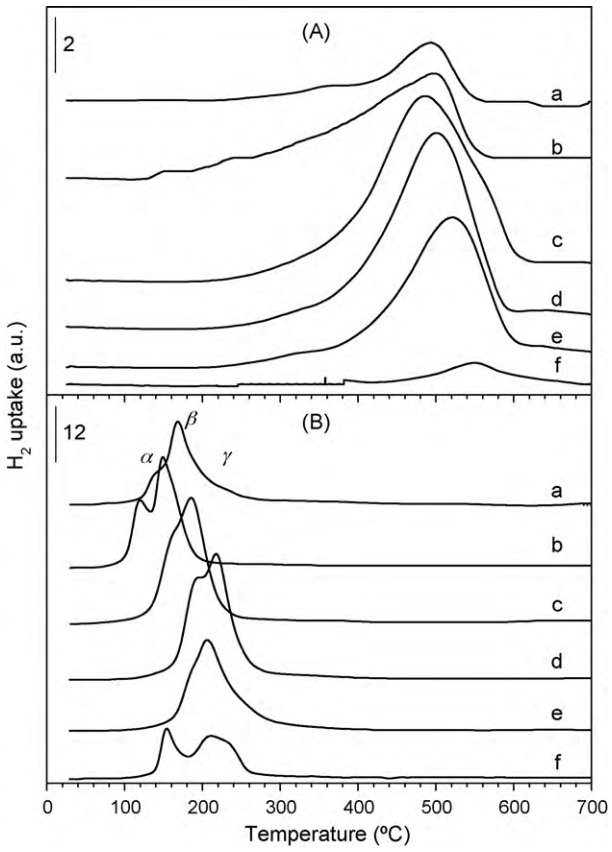

Fig. 9. H_2-TPR profiles of (A) $Ce_{1-x}Ti_xO_2$ supports and (B) $CuO/Ce_{1-x}Ti_xO_2$ catalysts calcined at 500 °C with the Ti/(Ce + Ti) atomic ratio x being (a) 0.0, (b) 0.2, (c) 0.4, (d) 0.6, (e) 0.8, and (f) 1.0.

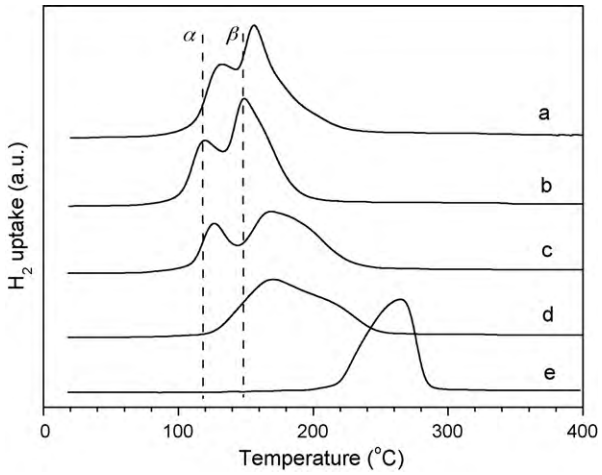

Fig. 10. H_2-TPR profiles of the $CuO/Ce_{0.8}Ti_{0.2}O_2$ catalysts calcined at (a) 400, (b) 500, (c) 600, (d) 700, and (e) 800 °C.

β. The catalyst $CuO/Ce_{0.8}Ti_{0.2}O_2$ exhibits the lowest reduction temperatures centered at 121 and 155 °C, while the other three catalysts (x = 0.4, 0.6, and 0.8) show the reduction peaks at higher temperature (above 167 °C).

H_2-TPR has been widely used to characterize the reduction property of CuO/CeO_2 entity. Liu et al. [17,55] reported four types of CuO species in CuO/CeO_2 catalysts: (I) isolated Cu^{2+} ions that interact strongly with the support; (II) weak magnetic associates of several Cu^{2+} ions that have close contact with each other; (III) small two- and three-dimensional clusters of loose structures that have no specific and regular lattice arrangement; (IV) large three-dimensional clusters and bulk CuO phase that have characters and properties identical to those of pure CuO powder. They ascribed the H_2-TPR peak α at lower temperature (ca. 176 °C) to the types (I) and (II) copper ions and peak β at higher temperature (ca. 196 °C) to type (III) CuO particles. A similar conclusion is also drawn by Avgouropoulos and Ioannides [16] and Luo et al. [56]; they ascribed peak α to finely dispersed CuO in close interacting with ceria and peak β to "bulk-like" CuO particles. Recently, Luo et al. [57] provided another explanation to the H_2-TPR of CuO-CeO_2 catalysts prepared by a surfactant-templated method; they attributed the three reduction peaks in the region of 150–280 °C to finely dispersed CuO, Cu^{2+} ions in $Cu_xCe_{1-x}O_{2-\delta}$ solid solution, and bulk CuO in turn. In these reports, however, the possible reduction of CeO_2 in the support is not considered.

From the quantitative results listed in Table 4, it is noticed that the amount of hydrogen consumption of the catalysts during TPR exceeds that required for the reduction of CuO to Cu (1257 μmol/g). Combining with the disappearance of the TPR peaks at higher temperatures (above 480 °C) ascribed to the reduction of the $Ce_{1-x}Ti_xO_2$ supports, it is deduced that the excessive amount of hydrogen consumed in TPR may be attributed to the reduction of the surface oxygen of CeO_2 in the Ce-containing catalysts or for the nonstoichiometric reduction of TiO_2 in CuO/TiO_2 catalyst. This conclusion is consistent with that observed by Tang et al. [58,59]. They found three reduction peaks at 130, 163 and 204 °C on the CuO/CeO_2 catalyst, which were ascribed to the amorphous CuO clusters closely interacting with CeO_2, the bulk-like CuO and the surface CeO_2, and the segregated CuO crystalline, respectively. Pintar et al. [60] also reported the similar observation that the excessive consumption of H_2 in TPR should be attributed to the amount of H_2 incorporated in the catalyst structure. In this respect, it is supposed that the peak α in the H_2-TPR profiles illustrated in Fig. 9B is ascribed to the highly dispersed CuO species strongly interacted with the support, peak β maybe corresponds to the reduction of CuO species with larger crystallite size and of the surface lattice oxygen of CeO_2 or TiO_2 supports, and peak γ may be attributed to the bulk CuO.

Comparing the reduction behavior of the catalysts with that of the supports, it is noticed that the reducing degree of CeO_2 and TiO_2 in the catalysts is similar to that in the corresponding supports, indicating that an interaction is present between CuO species and the surface oxygen of the supports. The reduction of the reducible part of CeO_2 and TiO_2 in the catalysts $CuO/Ce_{1-x}Ti_xO_2$ occurs at much lower temperature than that in the supports $Ce_{1-x}Ti_xO_2$, demonstrating an synergistic interaction that promotes both the reduction of CuO species and the reduction of CeO_2 or TiO_2 [40,41]. The catalyst $CuO/Ce_{0.8}Ti_{0.2}O_2$ exhibits the lowest reduction temperatures among all the catalysts tested. In fact, the lower reduction temperature indicates the presence of a strong interaction between CuO species and the support, which is closely related to the properties of CuO interfacial species and the nature of the supports. As mentioned before, the nature of the support is varied with Ce/Ti ratios, which has been confirmed by XRD and TEM. Therefore, the change of the reduction temperature also reflects the interaction between CeO_2 and TiO_2 in the support. Hornés et al. [61] also found similar phenomena in the CO-TPR study of $CuO/Ce_{1-x}Tb_xO_{2-y}$ (x = 0, 0.2 and 0.5); they supposed that the position of the reduction peak in TPR was related to the CuO interfacial properties and the nature of the support. As revealed by the XRD results, $CuO/Ce_{0.8}Ti_{0.2}O_2$ possesses the smallest CeO_2 cell unit parameters (Table 2), indicating the onset of a strong interaction between CeO_2 and TiO_2 and the formation of TiO_2–CeO_2 solid solution, where Ce–O bond is weakened and the interaction between CuO species and CeO_2 is enhanced. This may contribute to the high catalytic activity of $CuO/Ce_{0.8}Ti_{0.2}O_2$ catalyst.

Fig. 10 shows the H_2-TPR profiles of $CuO/Ce_{0.8}Ti_{0.2}O_2$ catalysts calcined at different temperatures. The catalyst calcined at 500 °C exhibits the lowest reduction temperature. The XRD results (Table 3) also revealed that the optimum calcination temperature for the formation of the TiO_2–CeO_2 solid solution is 500 °C. The strong interaction between CuO and the support for $CuO/Ce_{0.8}Ti_{0.2}O_2$ calcined at 500 °C leads to the decrease of the reduction temperature of both CuO and CeO_2 in the catalyst. When the calcination temperature exceeds 700 °C, the catalyst is severely sintered; two H_2 consumption peaks (α and β) are merged into a single peak and the reduction temperature shifts significantly to higher value.

4. Conclusions

A series of $CuO/Ce_{1-x}Ti_xO_2$ catalysts prepared by sol–gel impregnation was used as the catalysts for CO PROX. Their catalytic performance is related to support composition and calcination temperature. The catalyst $CuO/Ce_{0.8}Ti_{0.2}O_2$ exhibits the highest activity and the optimal calcination temperature is 500 °C.

The presence of H_2O and CO_2 in the reaction stream has a negative effect on the activity and stability of the catalyst $CuO/Ce_{0.8}Ti_{0.2}O_2$ for CO PROX. When the feed stream contains 10% H_2O and 15% CO_2, the temperature for a complete conversion of CO is raised by 40–50 °C compared with the feed free of H_2O and CO_2. Moreover, the negative effect of CO_2 on the catalyst stability is stronger than that of H_2O, suggesting that the accumulation of carbonate species may be the main reason for catalyst deactivation.

$CuO/Ce_{1-x}Ti_xO_2$ catalysts exhibit higher surface area, smaller particle size, and more highly dispersed copper species than CuO supported on pure CeO_2 or TiO_2. The strong interaction between TiO_2 and CeO_2 in the support revealed by XRD as well as the interfacial interaction between CuO and the support demonstrated by H_2-TPR may contribute to the high catalytic activity of $CuO/Ce_{0.8}Ti_{0.2}O_2$.

Acknowledgments

The authors are grateful for the financial support of the State Key Fundamental Research Project and the Natural Science Foundation of China (20773155) and Shanxi Province (2007011037).

References

[1] H. Tanaka, M. Kuriyama, Y. Ishida, S.I. Ito, K. Tomishige, K. Kunimori, Appl. Catal. A 343 (2008) 117.
[2] O. Pozdnyakova, D. Teschner, A. Wootsch, J. Kröhnert, B. Steinhauer, H. Sauer, L. Toth, F.C. Jentoft, A. Knop-Gericke, Z. Paál, R. Schlögl, J. Catal. 237 (2006) 17.
[3] S.Y. Chin, O.S. Alexeev, M.D. Amiridis, Appl. Catal. A 286 (2005) 157.
[4] Y.F. Han, M.J. Kahlich, M. Kinne, R.J. Behm, Appl. Catal. B 50 (2004) 209.
[5] L.H. Chang, N. Sasirekha, Y.W. Chen, Catal. Commun. 8 (2007) 1702.
[6] W. Deng, J. De Jesus, H. Saltsburg, M. Flytzani-Stephanopoulos, Appl. Catal. A 291 (2005) 126.
[7] H. Wang, H.Q. Zhu, Z.F. Qin, G.F. Wang, F.X. Liang, J.G. Wang, Catal. Commun. 9 (2008) 1487.
[8] H. Wang, H.Q. Zhu, Z.F. Qin, F.X. Liang, G.F. Wang, J.G. Wang, J. Catal. 264 (2009) 154.
[9] Y. Teng, H. Sakurai, A. Ueda, T. Kobayashi, Int. J. Hydrogen Energy 24 (1999) 355.
[10] Q. Guo, Y. Liu, Appl. Catal. B 82 (2008) 19.
[11] M. Kang, M.W. Song, C.H. Lee, Appl. Catal. A 251 (2003) 143.
[12] G. Avgouropoulos, T. Ioannides, Ch. Papadopoulou, J. Batista, S. Hocevar, H.K. Matralis, Catal. Today 75 (2002) 157.
[13] C.K. Costello, M.C. Kung, H.S. Oh, Y. Wang, H.H. Kung, Appl. Catal. A 232 (2002) 159.
[14] S.S. Pansare, A. Sirijaruphan, J.G. Goodwin, J. Catal. 234 (2005) 151.
[15] W. Liu, M. Flytzani-Stephanopoulos, J. Catal. 153 (1995) 304.
[16] G. Avgouropoulos, T. Ioannides, Appl. Catal. B 67 (2006) 1.
[17] Z.G. Liu, R.X. Zhou, X.M. Zheng, Catal. Commun. 9 (2008) 2183.
[18] A.M.D. de Farias, A.P.M.G. Barandas, R.F. Perez, M.A. Fraga, J. Power Sources 165 (2007) 854.
[19] D.H. Kim, J.E. Cha, Catal. Lett. 86 (2003) 107.
[20] G. Avgouropoulos, T. Ioannides, Appl. Catal. A 244 (2003) 155.
[21] F. Mariño, B. Schönbrod, M. Moreno, M. Jobbágy, G. Baronetti, M. Laborde, Catal. Today 133–135 (2008) 735.
[22] C.R. Jung, J. Han, S.W. Nam, T.H. Lim, S.A. Hong, H.I. Lee, Catal. Today 93–95 (2004) 183.
[23] P.V. Snytnikov, M.M. Popova, Y. Men, E.V. Rebrov, G. Kolb, V. Hessel, J.C. Schouten, V.A. Sobyanin, Appl. Catal. A 350 (2008) 53.
[24] R. Lin, M.F. Luo, Y.J. Zhong, Z.L. Yan, G.Y. Liu, W.P. Liu, Appl. Catal. A 255 (2003) 331.
[25] Y.Z. Chen, B.J. Liaw, C.W. Huang, Appl. Catal. A 302 (2006) 168.
[26] Y.Z. Chen, B.J. Liaw, H.C. Chen, Int. J. Hydrogen Energy 31 (2006) 427.
[27] Y.Z. Chen, B.J. Liaw, W.C. Chang, C.T. Huang, Int. J. Hydrogen Energy 32 (2007) 4550.
[28] P. Ratnasamy, D. Srinivas, C.V.V. Satyanarayana, P. Manikandan, R.S. Senthil Kumaran, M. Sachin, V.N. Shetti, J. Catal. 221 (2004) 455.
[29] A. Martínez-Arias, A.B. Hungría, M. Fernández-García, J.C. Conesa, G. Munuera, J. Power Sources 151 (2005) 32.
[30] M. Manzoli, R.D. Monte, F. Boccuzzi, S. Coluccia, J. Kašpar, Appl. Catal. B 61 (2005) 192.
[31] T. Caputo, R. Pirone, G. Russo, Kinet. Catal. 47 (2006) 756.
[32] M.F. Luo, J. Chen, L.S. Chen, J.Q. Lu, Z.C. Feng, C. Li, Chem. Mater. 13 (2001) 197.
[33] J. Rynkowski, J. Farbotko, R. Touroude, L. Hilaire, Appl. Catal. A 203 (2006) 335.
[34] T. López, F. Rojas, R. Alexander-Katz, F. Galindo, A. Balankin, A. Bulian, J. Solid State Chem. 177 (2004) 1873.
[35] J.L. Ye, Y.Q. Wang, Y. Liu, H. Wang, Int. J. Hydrogen Energy 33 (2008) 6602.
[36] Y. Zhang, Z.X. Li, X.B. Wen, Y. Liu, Chem. Eng. J. 121 (2006) 115.
[37] C. Gennequin, M. Lamallem, R. Cousin, S. Siffert, F. Aïssi, A. Aboukaïs, Catal. Today 122 (2007) 301.
[38] A.M.T. Silva, C.G. Silva, G. Dražić, J.L. Faria, Catal. Today 144 (2009) 13.
[39] G.L. Dong, J.G. Wang, Y.B. Gao, S.Y. Chen, Catal. Lett. 58 (1999) 37.
[40] H.Q. Zhu, Z.F. Qin, W.J. Shan, W.J. Shen, J.G. Wang, J. Catal. 225 (2004) 267.
[41] H.Q. Zhu, Z.F. Qin, J.G. Wang, Chin. J. Catal. 26 (2005) 377.
[42] H.Q. Zhu, Z.F. Qin, J.G. Wang, J. Fuel Chem. Technol. 32 (2004) 729.
[43] H.Q. Zhu, Z.F. Qin, W.J. Shan, W.J. Shen, J.G. Wang, J. Catal. 233 (2005) 41.
[44] H.Q. Zhu, Z.F. Qin, W.J. Shan, W.J. Shen, J.G. Wang, Catal. Today 126 (2007) 382.
[45] F.X. Liang, H.Q. Zhu, Z.F. Qin, G.F. Wang, J.G. Wang, Catal. Commun. 10 (2008) 737.
[46] F.X. Liang, H.Q. Zhu, Z.F. Qin, H. Wang, G.F. Wang, J.G. Wang, Catal. Lett. 126 (2008) 353.
[47] P. Sangeetha, Y.W. Chen, Int. J. Hydrogen Energy 34 (2009) 7342.
[48] J.W. Park, J.H. Jeong, W.L. Yoon, Y.W. Rhee, J. Power Sources 132 (2004) 18.
[49] D. Gamarra, A. Martínez-Arias, J. Catal. 263 (2009) 189.
[50] G. Sedmak, S. Hočevar, J. Levec, J. Catal. 213 (2003) 135.
[51] A. Martínez-Arias, A.B. Hungría, G. Munuera, D. Gamarra, Appl. Catal. B 65 (2006) 207.
[52] J. Fang, X.Z. Bi, D.J. Si, Z.Q. Jiang, W.X. Huang, Appl. Surf. Sci. 253 (2007) 8952.
[53] Z.Q. Zou, M. Meng, L.H. Guo, Y.Q. Zha, J. Hazard. Mater. 163 (2008) 835.
[54] X.F. Dong, H.B. Zou, W.M. Lin, Int. J. Hydrogen Energy 31 (2006) 2337.
[55] Z.G. Liu, R.X. Zhou, X.M. Zheng, J. Mol. Catal. A 255 (2006) 103.
[56] M.F. Luo, Y.J. Zhong, X.X. Yuan, X.M. Zheng, Appl. Catal. A 162 (1997) 121.
[57] M.F. Luo, J.M. Ma, J.Q. Lu, Y.P. Song, Y.J. Wang, J. Catal. 246 (2007) 52.
[58] X.L. Tang, B.C. Zhang, Y. Li, Y.D. Xu, Q. Xin, W.J. Shen, Appl. Catal. A 288 (2005) 116.
[59] X.L. Tang, B.C. Zhang, Y. Li, Y.D. Xu, Q. Xin, W.J. Shen, Catal. Today 93–95 (2004) 191.
[60] A. Pintar, J. Batista, S. Hočevar, J. Colloid Interface Sci. 285 (2005) 218.
[61] A. Hornés, P. Bera, A. López-Cámara, D. Gamarra, G. Munuera, A. Martínez-Arias, J. Catal. 268 (2009) 367.